
Constraints on the dark mass distribution surrounding Sgr A*: simple χ^2 analysis for the redshift of photons from orbiting stars

Yohsuke TAKAMORI,^{1*} Shogo NISHIYAMA,² Takayuki OHGAMI,³ Hiromi SAIDA,⁴ Rio SAITOU,⁴ Masaaki TAKAHASHI,⁵

¹National Institute of Technology (KOSEN), Wakayama College, Gobo, Wakayama 644-0023, Japan

²Miyagi University of Education, Sendai, Miyagi 980-0845, Japan

³Konan University, Kobe, Hyogo 658-8501, Japan

⁴Daido University, Naogya, Aichi 457-8530, Japan

⁵Aichi University of Education, Kariya, Aichi 448-8542, Japan

*E-mail: takamori@wakayama-nct.ac.jp

Received (reception date); Accepted (acceptation date)

Abstract

Sagittarius A* (Sgr A*) is the central supermassive black hole with the mass $\sim 4 \times 10^6 M_\odot$ in the Milky Way and stars are orbiting around it. In May 2018, one of the nearest stars to Sgr A* named S0-2/S2 experienced the pericenter passage. The redshift of photons from S0-2 had varied from 4000 km s^{-1} to -2000 km s^{-1} during the pericenter passage, which is within 0.5 yr. In this paper, we show that this steep variation of the redshift gives a strong constraint on a dark mass distribution inside the orbit of S0-2. By applying a simple χ^2 analysis to the observed redshift, we can easily distinguish between the two models, the point mass model and the point mass plus an extended mass model without the best-fitting parameter search. Our redshift data during the pericenter passage in 2018 with Subaru/IRCS bound the amount of the extended mass inside the orbit of S0-2 less than 0.5% ($\sim 2 \times 10^4 M_\odot$) of the mass of Sgr A*. This constraint obtained by our simple analysis is comparable to previous works with the best-fitting parameter search to the motion of S0-2 including the effect of the extended mass. We consider both the power-law and the Plummer models for the dark mass distribution model, but the significant difference between these results is not found.

Key words: black hole physics — gravitation — Galaxy: center

1 Introduction

Sagittarius A* (Sgr A*) is a radio source which locates at the center of the Milky Way. Astronomers have been observing around Sgr A* over the past few decades and found that stars move around it. The stars, which are called S-stars, tell us that Sgr A* is a supermassive black hole whose mass is about $4 \times 10^6 M_\odot$ (see the latest research: GRAVITY collab. 2018; Do et al. 2019; Saida et

al. 2019; GRAVITY collab. 2020). In 2018, we had a big event for Sgr A*. One of the nearest S-stars to Sgr A* named S0-2/S2 (hereafter we call it S0-2), experienced the pericenter passage (the distance from Sgr A* is about 120 au) in the year. Astronomers expect that this big event gives us new information to test Einstein's gravity theory in the environment around a supermassive black hole. Three telescopes, which are Keck observatory, Very Large Telescope (VLT), and Subaru telescope, have been ready

to observe that big event in 2018 independently. Keck and VLT can carry out both astrometric and spectroscopic measurements for S-stars (e.g., Boehle et al. 2016; Gillessen et al. 2017). Subaru telescope can perform high-resolution spectroscopic measurements with IRCS (Nishiyama et al. 2018). As a result of their astrometric/spectroscopic observations in 2018, they found that S0-2 experienced the pericenter passage in May 2018. Moreover, they showed that the spectroscopic measurements of S0-2 during the pericenter passage strongly suggest that Einstein’s gravity is preferable to Newton’s gravity in the environment around a supermassive black hole (GRAVITY collab. 2018; Do et al. 2019). In addition to these works, Saida et al. (2019) has pointed out another view of the “general relativistic effect” within the spectroscopic data obtained by Subaru/IRCS during the pericenter passage of S0-2 in 2018. Recently, GRAVITY collab. (2020) has performed the orbital fitting to the motion of S0-2 with the data up to the end of 2019 and reported that they caught the general relativistic pericenter shift in the data.

The present observational data of S0-2 are well explained under the assumption that S0-2 feels only the gravity from Sgr A*. However, within the uncertainties of the observational data, the deviation from the above assumption can be examined. As one possibility of such deviation, we consider a dark mass distribution surrounding Sgr A*, e.g., faint S-stars, neutron stars, stellar mass black holes, faint accretion gas clouds, and a dark matter. The amount of such dark extended mass has been bounded within the uncertainties of the observational data. Before the pericenter passage of S0-2 in 2018, the acceptable amount of the extended mass inside the orbit of S0-2 is 1% of the mass of Sgr A* at most (Boehle et al. 2016; Gillessen et al. 2017). After the observations of S0-2 in 2018, GRAVITY collab. (2018) reported that the acceptable extended mass is in the range 0.35%–1% depending on the extended mass models, though they did not show their observed data and the detail of their analysis. Do et al. (2019) performed the Bayesian parameter estimation for the motion of S0-2 including the profile of the dark mass distribution. As a result, they obtained the absolute mass of the extended mass within the orbit of S0-2, which is $5.5 \times 10^3 M_\odot / 12.7 \times 10^3 M_\odot$ with $1\sigma/2\sigma$. Converting into the percentage with $M_{\text{BH}} = 4 \times 10^6 M_\odot$, it is in the range 0.14%–0.32%. Moreover, GRAVITY collab. (2020) showed that the upper limit of the extended mass inside the orbit of S0-2 is $\sim 0.1\%$ ($\sim 4 \times 10^3 M_\odot$) of Sgr A* with 1σ .

In the previous papers (GRAVITY collab. 2018; Do et al. 2019; GRAVITY collab. 2020), they have given the upper limits of the amount of the extended mass by perform-

ing the best-fit parameter search for the motion of S0-2 and Sgr A* including a dark mass distribution with their astrometric and spectroscopic data of S0-2 during the pericenter passage in 2018. In this paper, we focus on the spectroscopic data of S0-2 and show that the data during the pericenter passage give a strong constraint on the amount of the extended mass inside the orbit of S0-2. The spectroscopic data tell us the redshift of photons from S0-2. From the observation of S0-2 during the pericenter passage in 2018, we can see that the redshift had varied from 4000 km s^{-1} to -2000 km s^{-1} within 0.5 yr. Thanks to this steep variation of the redshift, we can easily distinguish the two models, the point mass model and the point mass plus an extended mass model. The aims of this paper are as follows:

- (i) Propose a simple χ^2 analysis which needs much less numerical costs compared with the method used in the previous papers (Do et al. 2019; GRAVITY collab. 2020), and give a constraint on a dark mass distribution around Sgr A*.
- (ii) Show our spectroscopic data obtained by Subaru/IRCS during the pericenter passage of S0-2 in 2018 can give a strong constraint on the amount of the extended mass inside the orbit of S0-2 by using the χ^2 analysis proposed in (i).

We do *not* perform the best-fitting parameter search including a dark mass distribution which needs much numerical cost (GRAVITY collab. 2018; Do et al. 2019; GRAVITY collab. 2020). Instead of the best-fitting parameter search, we suggest a simple χ^2 analysis with spectroscopic data. The procedure of our χ^2 analysis is as follows. We solve the equation of motion of a S-star in two cases of the point mass and the point mass plus an extended mass models. Then, we calculate the value of χ^2 with spectroscopic data for the motion of the S-star in both models and take the ratio of those χ^2 . Our method relies on the fact that the present observational data are well explained by the point mass model, and the effect of the extended mass can be regarded as a small perturbation within the uncertainties of observed data. The ratio of χ^2 becomes an indicator whether the dark mass distribution model is acceptable. For S0-2, the time evolution of the redshift had varied from 4000 km s^{-1} to -2000 km s^{-1} during the pericenter passage, which is within 0.5 yr. Thanks to this steep variation of the redshift, we can infer how much mass for the dark extended object is acceptable. By applying our χ^2 analysis to our work Saida et al. (2019), we find that the amount of the extended mass inside the orbit of S0-2 is less than 0.5% ($\sim 2 \times 10^4 M_\odot$) of Sgr A*. Our result is stronger by the factor 1/2 than the

results obtained before the pericenter passage (Boehle et al. 2016; Gillessen et al. 2017). This constraint is comparable to the recent works including the data during the pericenter passage in 2018 (GRAVITY collab. 2018; Do et al. 2019; GRAVITY collab. 2020). In GRAVITY collab. (2018) and Do et al. 2019, they considered the power-law model (Ghez et al. 2008; Boehle et al. 2016; Gillessen et al. 2017) for the dark mass distribution which represents a stellar cluster and is supported by the surface brightness of the galactic center region with infrared observations (Genzel et al. 2003; Schödel et al. 2007). In addition to that model, we also adopt a Plummer model (Rubilar & Eckart 2001; Mouawad et al. 2005; Gillessen et al. 2009; GRAVITY collab. 2020) for the dark mass distribution. The Plummer model is applied initially to a globular cluster (Plummer 1911) and is available for a dark mass distribution model around Sgr A*. Although we consider these two models, we do not find a significant difference between those results.

This paper is organized as follows. In section 2, we introduce the equation of motion of an orbiting star around Sgr A* in the post-Newtonian treatment in the context of the general relativity. Moreover, we introduce two dark mass distribution models: the power-law model; the Plummer model. In section 3, we discuss the influence of the dark mass distribution on the redshift of photons from S0-2. The dark mass distribution affects the timing of the pericenter passage. It plays an important role to give a strong constraint on the dark mass distribution. In section 4, we explain our χ^2 analysis to the observed redshift of S0-2. We can easily distinguish the point mass model and the point mass plus an extended mass model with our method. As a result, we obtain the upper limit of the amount of the extended mass, which is 0.5% of Sgr A*. The last section is devoted to the summary and discussion. Through this paper, c and G represent the speed of light and Newton's gravity constant, respectively.

2 Equation of motion of an orbiting star and dark extended mass models

2.1 Equation of motion of an orbiting star in the post-Newtonian approximation

We calculate the motion of an orbiting star around Sgr A* based on general relativity. Since S-star's orbits are far from Sgr A*(even the periapsis distance of S0-2 is about 2000 times the size of the central black hole), we do not need full general relativistic treatment. In the case of S0-2, the post-Newtonian approximation is available. The equation of motion of a free test particle around a central

object with mass M can be written as

$$\frac{d^2 \mathbf{r}}{dt^2} = -\frac{GM}{r^3} \mathbf{r} + \frac{GM}{c^2 r^3} \left(\frac{4GM}{r} - v^2 \right) \mathbf{r} + \frac{4GM \mathbf{r} \cdot \mathbf{v}}{c^2 r^3} \mathbf{v}, \quad (1)$$

where \mathbf{r} is the position vector of the test particle with respect to the central object, and \mathbf{v} is its velocity. Then, r and v are the absolute value of \mathbf{r} and \mathbf{v} , respectively. The first term on the right-hand side is Newton's gravity and the others are the general relativistic effects. We need to include influence from a dark mass distribution surrounding Sgr A* to equation (1). The most simple deformation is making the mass M be a function of \mathbf{r} , that is $M \rightarrow M(\mathbf{r})$ (Rubilar & Eckart 2001). This deformation would be enough to express a small mass fraction surrounding Sgr A*. We apply equation (1) with $M(\mathbf{r})$ to the dynamics of S0-2 and solve it numerically.

2.2 Point mass plus an extended mass model

Various possibilities are available for a dark mass distribution surrounding Sgr A*. In this paper, we mainly focus on a stellar cluster model based on the surface number density of stars near Sgr A* by infrared observation (Genzel et al. 2003; Schödel et al. 2007). We consider two models representing a spherically symmetric mass distribution; the power-law model (Ghez et al. 2008; Boehle et al. 2016; Gillessen et al. 2017; GRAVITY collab. 2018; Do et al. 2019) and the Plummer model (Rubilar & Eckart 2001; Mouawad et al. 2005; Gillessen et al. 2009; GRAVITY collab. 2020). We briefly summarize these models here.

Let us show the power-law model at first. The enclosed mass $M(r)$ with the mass density proportional to $r^{-\gamma}$ can be written as

$$M(r) = \begin{cases} M_{\text{tot}} \left\{ 1 - \eta + \eta \left(\frac{r}{r_c} \right)^{3-\gamma} \right\}, & (r \leq r_c); \\ M_{\text{tot}}, & (r > r_c), \end{cases} \quad (2)$$

where M_{tot} is the total mass of the central black hole and the dark mass distribution within r_c and η ($0 \leq \eta < 1$) is the ratio of the amount of the extended mass to the mass of the central black hole. Then, the mass of the central black hole is given by $M_{\text{BH}} = (1 - \eta)M_{\text{tot}}$. The power-law slope γ is taken as 2.5 in GRAVITY collab. (2018) or as 1.5 in Do et al. (2019). Ghez et al. (2008) showed that the extended mass upper limit did not depend strongly on the value of γ in the range from 0.5 to 3. In this paper, we choose γ to be 1.5 as in Do et al. (2019). Since the cutoff radius is taken as $r_c = 0.011$ pc in Do et al. (2019), we also use 0.011 pc for r_c .¹

Next, let us show the Plummer model which is applied

¹ Boehle et al. (2016) set the cutoff radius to $r_c = 0.011$ pc, such that it encloses the orbits of S0-2 and S0-38.

initially to a globular cluster (Plummer 1911). The mass function of the Plummer model is given by

$$M(r) = M_{\text{tot}} \left(1 - \eta + \eta \frac{\int_0^r \tilde{\rho}(\xi) \xi^2 d\xi}{\int_0^{r_0} \tilde{\rho}(\xi) \xi^2 d\xi} \right), \quad (3)$$

where r_0 is a parameter which makes M_{tot} be the total mass within r_0 . Then, $\tilde{\rho}$ is the mass density function written as

$$\tilde{\rho}(r) = \left\{ 1 + \left(\frac{r}{r_c} \right)^2 \right\}^{-5/2}. \quad (4)$$

r_c gives the clumping scale of the model. Since we are interested in the motion of S0-2, we take r_0 as the apoapsis distance of S0-2 (~ 0.01 pc). In Mouawad et al. (2005), they constructed a multi Plummer profile, and the most inner core has that $r_c = 0.015$ pc, and therefore we use it for our calculation.

Taking $\eta = 0$, both the power-law and the Plummer models revisit the point mass model with $M_{\text{BH}} = M_{\text{tot}}$. It is worth to show the mass density profiles of the power-law and the Plummer models. The mass density profile for a spherically symmetric mass distribution is given by

$$\rho(r) = \frac{1}{4\pi r^2} \frac{dM}{dr}. \quad (5)$$

For the power-law model, we have

$$\rho(r) = \frac{\eta M_{\text{tot}}}{4\pi r_c^3 (3 - \gamma)} \left(\frac{r}{r_c} \right)^{-\gamma}. \quad (6)$$

Then, the mass density function of the Plummer model is given by

$$\rho(r) = \frac{\eta M_{\text{tot}}}{4\pi \int_0^{r_0} \tilde{\rho}(\xi) \xi^2 d\xi} \left\{ 1 + \left(\frac{r}{r_c} \right)^2 \right\}^{-5/2}. \quad (7)$$

We show the mass density profiles of the power-law and the Plummer models in figure 1. Moreover, we also show the mass functions in the case of $\eta = 0.01$ in figure 2.

3 Influence on the redshift due to a dark mass distribution

In this section, we discuss how a dark mass distribution affects the redshift of photons from S0-2. The velocity of S0-2 induced by a dark mass distribution with 1% of the mass of Sgr A* is about a tenth of the general relativistic effect (Preto & Saha 2009; Iorio 2011). Thus, one thinks that it would be difficult to detect the effect even if we get spectroscopic data of S0-2 during the pericenter passage. However, we should note that the existence of a dark mass distribution changes the timing of the pericenter passage because the mass affects the period of the star. Based on Kepler's third law, we can estimate that the change of the period due to the dark mass is ~ 0.01 yr. For S0-2, the time evolution of redshift had varied from 4000 km s^{-1} to

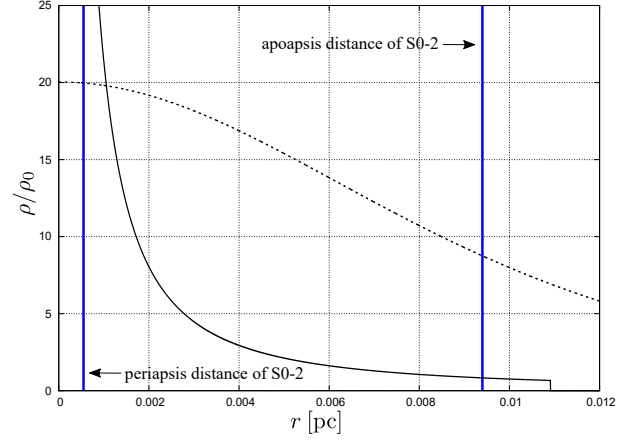


Fig. 1. The mass density profiles of the power-law and the Plummer models used in this paper. The mass density is normalized by $\rho_0 = \eta M_{\text{tot}} / (4\pi r_c^3)$. The solid and the dashed lines represent the mass density profiles of the power-law and the Plummer models. The horizontal axis shows the distance from the Galactic Center. We also show the periapsis, r_{peri} , and the apoapsis, r_{apo} , distances with the vertical lines. We calculate those with the parameters of S0-2 and Sgr A* in table 1 and obtain $r_{\text{peri}} = 5.5 \times 10^{-4}$ pc and $r_{\text{apo}} = 9.4 \times 10^{-3}$ pc. (Color online)

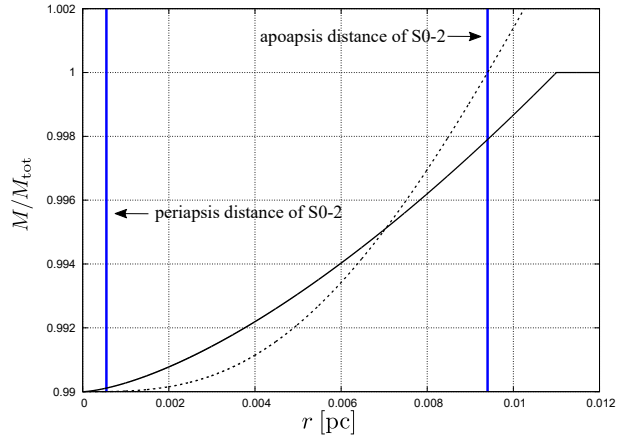


Fig. 2. The mass functions of the power-law and the Plummer model in the case of $\eta = 0.01$. The lines are drawn in the same manner in figure 1. Note that the radius giving M_{tot} is different between the power-law and the Plummer models here. For the power-law model, it is $r_c = 0.011$ pc that is the cutoff scale. For the Plummer model, it is $r_0 = 9.4 \times 10^{-3}$ pc that is the apoapsis distance of S0-2. (Color online)

-2000 km s^{-1} within 0.5 yr during the pericenter passage in 2018. From that, we can estimate the acceleration of S0-2 in the pericenter passage is of order $10^4 \text{ km s}^{-1} \text{ yr}^{-1}$. Because the timing of the pericenter passage can change 0.01 yr due to the dark mass, the velocity of S0-2 in the case of the point mass plus an extended mass model can change, roughly, $\sim 10^2 \text{ km s}^{-1}$ from the point mass model at the pericenter. We will show that the effect on the velocity of S0-2 by the dark mass distribution reaches 800 km s^{-1} during the pericenter passage.

3.1 Redshift in the post-Newtonian approximation

Let us introduce the redshift of photons from a moving star in the dark mass distribution in the context of the post-Newton approximation (Do et al. 2019). Taking our coordinate system as a cartesian (X, Y, Z) , and assuming the observer locates on the Z -axis and well far from the central black hole, the redshift measured at observation time t_{obs} is given by

$$z(t_{\text{obs}}) = \frac{v_Z(t_{\text{em}})}{c} + \frac{v(t_{\text{em}})^2}{2c^2} + \frac{GM(r(t_{\text{em}}))}{c^2 r(t_{\text{em}})} + \frac{v_{Z0}}{c}. \quad (8)$$

v_Z is the Z -component of the velocity of the star \mathbf{v} , and t_{em} is an emission time of a photon. The first term represents the radial velocity of the star. The second and the third terms are the transverse Doppler shift and the gravitational redshift, respectively. The fourth term is the Z -component of the solar system's velocity relative to Sgr A*. For the motion of photons from S0-2 to the observer, Minkowskian treatment is a good approximation because general relativistic effects such as the lensing are negligible yet. Then, with counting the Römer effect, we have the following relation between the observation time t_{obs} and the emission time t_{em} with eliminating the traveling time from the Galactic Center to the observer:

$$t_{\text{obs}} = t_{\text{em}} + \frac{Z(t_{\text{em}})}{c}, \quad (9)$$

where Z is the Z -component of the position vector of the star. We need to search the emission time t_{em} for given t_{obs} . Since $t_{\text{obs}} \sim 2010$ yr and $Z/c \sim 10$ days, it is sufficient to use the following relation for our purpose:

$$t_{\text{em}} = t_{\text{obs}} - \frac{Z(t_{\text{obs}})}{c}. \quad (10)$$

Combing equations (8) and (10), we can express a model of observed redshift.

3.2 Redshift in the point mass model and the point mass plus an extended mass model

We solve equation (1) numerically for the cases $\eta = 0$ (the point mass model) and $\eta \neq 0$ (the point mass plus an extended mass model). Because both the power-law model and the Plummer model have a similar effect on the time evolution of the redshift, we show the power-law model, for example. For the point mass model ($\eta = 0$), we take the orbital parameters of S0-2 and the parameters of Sgr A* from the general relativistic best-fitting parameter values given in Saida et al. (2019) (see the row named GR-best-fit in table 5 of the paper). The general relativistic best-fitting parameter values related to calculating the redshift are summarized in table 1. The initial position of S0-2 is set at the previous apocenter at 2010.3383. On the other hand, for

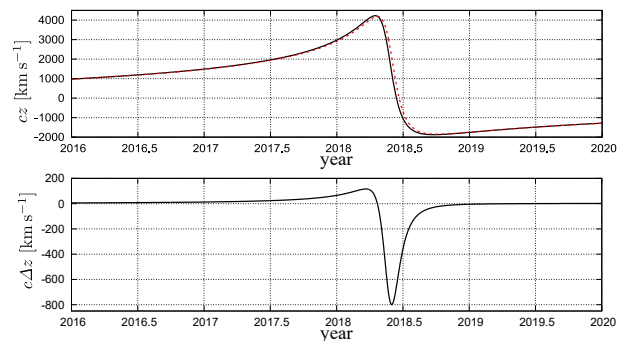


Fig. 3. The top panel shows the time evolution of the redshift. The solid line represents the case of the point mass model z_{PM} and the dashed line represents the case of the power-law model z_{PL} with $\eta = 0.01$. The bottom panel shows the discrepancy between the two models that is $\Delta z = z_{\text{PM}} - z_{\text{PL}}$. It becomes quite significant during the pericenter passage because of the difference in the timing of the pericenter passage. The max absolute value reaches 800 km s^{-1} in the case of $\eta = 0.01$. (Color online)

the power-law model ($\eta \neq 0$), we take the total mass and the fraction of the extended mass as $M_{\text{tot}} = 4.232 \times 10^6 M_{\odot}$ and $\eta = 0.01$, respectively, where M_{tot} is equal to the best-fitting parameter value of the mass of Sgr A* in the point mass model ($\eta = 0$). The initial conditions are taken as same as the case of the point mass model. The results are shown in figure 3. The discrepancy between the two models is quite large during the pericenter passage, which reaches 800 km s^{-1} . We can see that the timing of the maximum of redshift is slightly different between the cases $\eta = 0$ and $\eta \neq 0$. Moreover, the time evolution of the redshift shows the steep variation within about 0.5 yr. These cause the large discrepancy during the pericenter passage as shown in figure 3.

Table 1. Some of the general relativistic best-fitting parameter values of Sgr A* and S0-2 in Saida et al. (2019).

Parameters	Description	Value
$M_{\text{BH}} [10^6 M_{\odot}]$	Mass of Sgr A*	4.232
R_0 [kpc]	Distance to Sgr A*	8.098
$v_{Z0} [\text{km s}^{-1}]$	Relative velocity	-8.345
I [deg]	Inclination	134.239
Ω [deg]	Ascending node	227.766
ω [deg]	Argument of periapsis	66.204
e	Eccentricity	0.8903
T [yr]	Period	16.0504

4 Limit on the amount of the extended mass with a simple χ^2 analysis

We have seen from the figure 3 that a dark mass distribution affects the time evolution of redshift, and the influence is quite significant during the pericenter passage. It

can give us a strong constraint on a dark mass distribution around Sgr A*, and we will show that in this section. One of the main points of our paper is that we do not perform the best-fitting parameter search to the motion of S0-2 including the dark mass distribution which needs much numerical cost as in GRAVITY collab. (2018), Do et al. (2019), and GRAVITY collab. (2020). Instead of the best-fitting parameter search, we suggest a simple χ^2 analysis to the redshift of S0-2. The present observational data of S0-2 are well explained by the point mass model. Thus, the effect of the dark mass distribution to the motion of S0-2 can be regarded as a small perturbation within the uncertainties of the observed data. By applying our χ^2 analysis to the observed redshifts used in Saida et al. (2019), we can easily distinguish between the point mass model and the point mass plus an extended mass model thanks to the steep variation of the redshift during the pericenter passage. As a result, our χ^2 analysis gives a strong constraint on the amount of the extended mass, which is less than 0.5% ($\sim 2 \times 10^4 M_\odot$) of Sgr A*. Our results are comparable to the previous works with the best-fitting parameter search (GRAVITY collab. 2018; Do et al. 2019; GRAVITY collab. 2020). We will show our χ^2 analysis and the results here.

4.1 Simple χ^2 analysis

We calculate the χ^2 for the observed redshifts as

$$\chi^2 = \sum_{i=1}^N \frac{(z_i - z_{\text{model}}(t_i))^2}{\sigma_i^2}, \quad (11)$$

where z_i is the observed redshift with the uncertainty σ_i , $z_{\text{model}}(t_i)$ is a theoretical redshift at the observational time t_i and N is the total number of spectroscopic data. We have the general relativistic best-fitting model of the motion of S0-2 obtained by Saida et al. (2019), which corresponds to the case of $\eta = 0$. Moreover, the effect of the extended mass around Sgr A* (the case of $\eta \neq 0$) is allowed within the uncertainties of observational data. Therefore, we can distinguish these models by comparing χ^2 between the cases of $\eta = 0$ and $\eta \neq 0$. Here, let us introduce a normalized χ^2 defined by

$$\chi_n^2 := \frac{\chi_{\eta \neq 0}^2}{\chi_{\eta=0}^2}, \quad (12)$$

where $\chi_{\eta=0}^2$ and $\chi_{\eta \neq 0}^2$ are the values of χ^2 in the cases of $\eta = 0$ and $\eta \neq 0$, respectively. This normalized χ^2 shows the discrepancy between the point mass model ($\eta = 0$) and the point mass plus an extended mass model ($\eta \neq 0$). In our analysis, we use χ_n^2 to see whether the model with $\eta \neq 0$ is acceptable. To determine the acceptable value of χ_n^2 , we calculate χ_n^2 with the Newtonian model of S0-2's

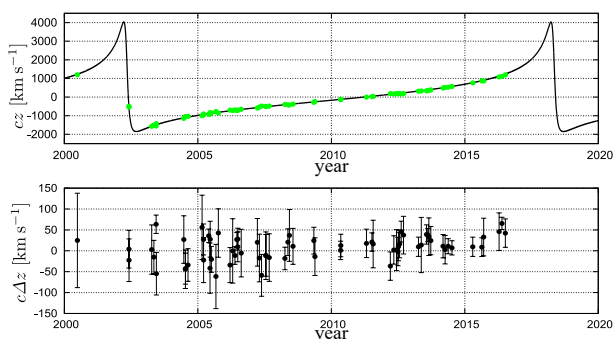
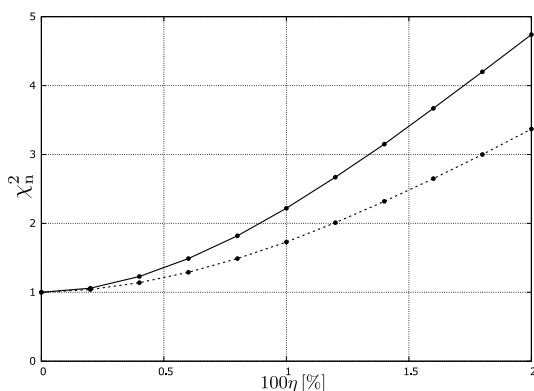
motion and the observed redshifts in Gillessen et al. (2017) where the spectroscopic data before the pericenter passage in 2018 are used. They have obtained the upper limit of the amount of the extended mass inside the orbit of S0-2 is 1% of Sgr A*. Therefore, by calculating χ_n^2 with their upper limit case, we can determine the acceptable upper limit of χ_n^2 based on the spectroscopic data before 2018. Then, we calculate χ_n^2 with the results in Saida et al. (2019) where the spectroscopic data during the pericenter passage in 2018 are included. Since the acceptable upper limit of χ_n^2 is determined based on the observed data before 2018, our analysis with the results in Saida et al. (2019) shows how the spectroscopic data during the pericenter passage in 2018 affect the constraint on the dark mass distribution.

4.2 Determination of the acceptable χ_n^2 with the observed redshifts before the pericenter passage in 2018

To determine the acceptable range of χ_n^2 , we calculate χ_n^2 with the results in Gillessen et al. (2017). They have performed an orbital fitting method to the motion of S0-2 in the context of Newton's gravity both in the point mass model and the point mass plus an extended mass model. Therefore, we solve equation (1) eliminating the 2nd and 3rd terms in the right-hand side with the parameters in the row 9 in table 1 and the row named S2 in table 3 in Gillessen et al. (2017). We summarize some of those parameters in table 2. We start our calculation from the previous apocenter, which is in 2010.33. Figure 4 shows the time evolution of the redshift in the case of $\eta = 0$ and the residual from the observed redshifts used in Gillessen et al. (2017). We calculate $\chi_{\eta=0}^2$ with those observed redshifts not including the observed data during the pericenter passage in 2018. Then, we also solve the equation of motion in the case of $\eta \neq 0$ with the initial conditions as same as the case of $\eta = 0$, and calculate $\chi_{\eta \neq 0}^2$ for various value of η . Then, we obtain χ_n^2 . The results are shown in figure 5. There is no significant difference between the power-law (the solid line with points in figure 5) and the Plummer (the dotted line with points in figure 5) models. In Gillessen et al. (2017), they concluded that the amount of the extended mass is 1% of Sgr A*, i.e., $\eta = 0.01$ at most. This corresponds to χ_n^2 of 1.7 to 2.2 in figure 5. Therefore, we can give the upper value of the acceptable range of χ_n^2 as $\chi_n^2 \sim 2.0$.

Table 2. Some of the best-fitting parameter values of Sgr A* and S0-2 in Gillessen et al. (2017).

Parameters	Description	Value
$M_{\text{BH}} [10^6 M_{\odot}]$	Mass of Sgr A*	4.28
R_0 [kpc]	Distance to Sgr A*	8.32
$v_{Z0} [\text{km s}^{-1}]$	Radial velocity of Sgr A*	14.2
I [deg]	Inclination	134.18
Ω [deg]	Accending node	226.94
ω [deg]	Argument of periapsis	65.51
e	Eccentricity	0.8839
T [yr]	Period	16.00


Fig. 4. The top panel shows the time evolution of redshift in the case of the point mass model ($\eta = 0$). We also show the observed redshifts from 2000–2016 shown in Gillessen et al. (2017) by the filled circles with error bars. The total number of the data, N , is 68. The bottom panel is the residual between the observed redshifts and the theoretical model. We can reproduce the time evolution of redshift shown in Gillessen et al. (2017) well. (Color online)

Fig. 5. χ_n^2 based on the results in Gillessen et al. (2017). The solid and dashed lines with points represent χ_n^2 the cases of the power-law and the Plummer models, respectively. We calculate χ_n^2 at the points and connect them with a line for the two models. There is no significant difference between them and 1% ($\eta = 0.01$) which is the upper limit in Gillessen et al. (2017) corresponds to $\chi_n^2 \sim 2.0$.

4.3 Limit on the amount of the extended mass including Subaru observational data during the pericenter passage in 2018

Let us calculate χ_n^2 with the results in Saida et al. (2019). They have found the general relativistic best-fitting orbital model of S0-2 using the astrometric and the spectroscopic data given in Boehle et al. (2016) and Gillessen et al. (2017) and the spectroscopic data obtained by Subaru/IRCS. We expect that the spectroscopic data during the pericenter passage in 2018 obtained by Subaru/IRCS would bound the amount of the extended mass more strongly than the bound given in Gillessen et al. (2017). We numerically solve equation (1) with the parameters in table 1 and calculate χ_n^2 for various η . The results are shown in figure 6. Obeying our criterion obtained in section 4.2 that is $\chi_n^2 \leq 2.0$, the acceptable fraction of the mass is about $100\eta \sim 0.5\% \sim 2 \times 10^4 M_{\odot}$ in the both models, which is a stronger constraint than that given in Gillessen et al. (2017).

To better understand our results, let us see the detail of the cases of $\eta = 0$ and $\eta = 0.01$. Since there is no significant difference between the power-law and the Plummer models, we only show the power-law model. Figure 7 shows the time evolution of redshift in the cases of $\eta = 0$ and $\eta = 0.01$ in the power-law model. The solid and the dashed lines represent the cases $\eta = 0$ and $\eta = 0.01$, respectively. The points with error bars represent the observed redshifts used in Saida et al. (2019). The filled circles (green) are the observed redshifts in Gillessen et al. (2017), and the open circles (blue) are those from Subaru/IRCS shown in Saida et al. (2019). We zoom that figure around the pericenter passage in 2018 and display it in figure 8. Moreover, we show the residual between the observed redshifts and the theoretical models in figure 9.

Our analysis shows that the redshift observations around the pericenter passage are crucial to constrain the amount of the extended mass around Sgr A*. As shown in figure 9, the redshift difference between $\eta = 0$ and $\eta = 0.01$ is very small between 2003 and 2017. On the other hand, the difference has become as large as 800 km s^{-1} in 2018, during the pericenter passage of S0-2. This significant difference was thus expected to be detected in the 2018 observations. By comparing the top and bottom panels in figure 9, we conclude that the extended mass with 1% of Sgr A* is excluded. The observed redshifts and the point mass model ($\eta = 0$) are consistent within 2σ (the top panel in figure 9). By contrast, the residuals between the observations and the point mass plus the extended mass model ($\eta = 0.01$) are more than several 100 km s^{-1} (bottom panel). It means that $\eta = 0.01$ model can not well reproduce the observed

redshifts. One of the reasons we can clearly differentiate the two models ($\eta = 0$ and $\eta = 0.01$) is that we could measure the redshift of S0-2 at 2018.38, the third data point from the right in figure 7–9. This is not the peak or bottom of the redshift, but it is close to the maximum point in the difference between the two models (the bottom panel in figure 3). It will be crucial to make observations at an appropriate time to give a stronger constraint on the amount of the extended mass and the mass density profile.

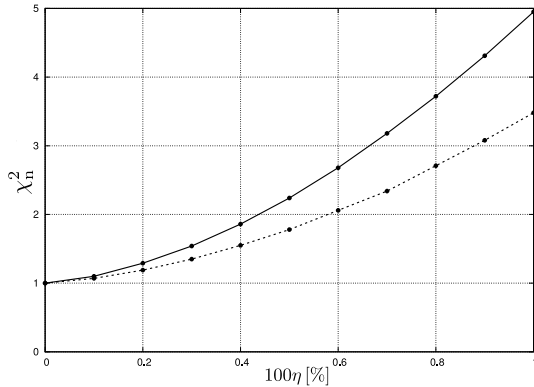


Fig. 6. χ_n^2 based on the results in Saida et al. (2019). The solid and dashed lines with points represent χ_n^2 in the cases of the power-law and the Plummer models, respectively. We calculate χ_n^2 at the points and connect them with a line for the two models. Focusing the case of $100\eta = 1\%$ which is acceptable in Gillessen et al. (2017), $\chi_n^2 > 3$ for the both models. Since the upper value of χ_n^2 obtained in section 4.2 is $\chi_n^2 \sim 2.0$, we exclude the case of $100\eta = 1\%$. It means that the acceptable amount of extended mass is bounded less than 1% of Sgr A* due to adding the data from Subaru/IRCS.

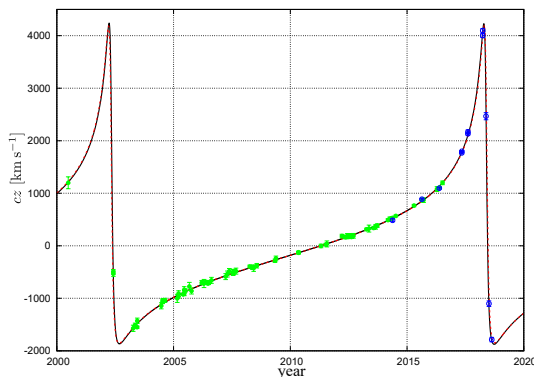


Fig. 7. The time evolution of redshift. The solid and dashed line represent the cases $\eta = 0$ and $\eta = 0.01$ in the power-law model, respectively. The points with error bars are the observed redshifts. The filled circles (green) are from Gillessen et al. (2017). The open circles (blue) are the data obtained by Subaru/IRCS (Saida et al. 2019). The total number of data, N , is 80. (Color online)

5 Summary and Discussion

The star S0-2 moving around Sgr A* passed through the pericenter in May 2018. We expect that this event gives

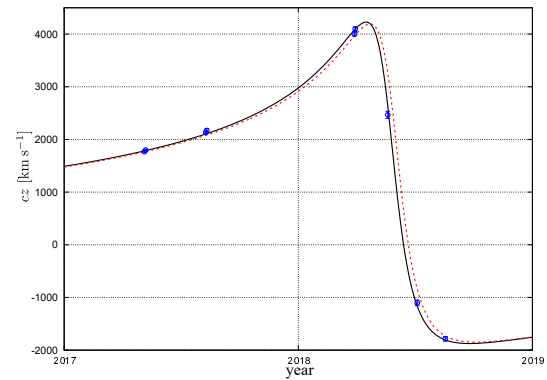


Fig. 8. The time evolution of redshift around the pericenter passage. We can see that the data points are well fitted in the case of $\eta = 0$ but the case of $\eta = 0.01$ is off the points during the pericenter passage. (Color online)

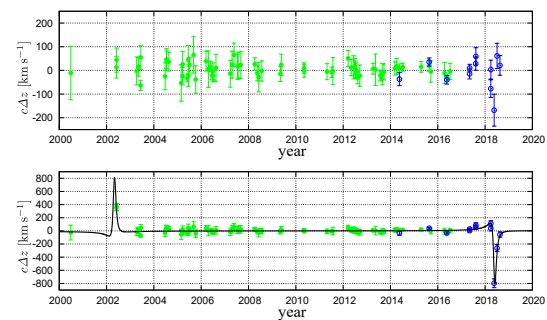


Fig. 9. The residual between the observed redshifts used in Saida et al. (2019) and the theoretical models. The top and the bottom panels show the cases of $\eta = 0$ and $\eta = 0.01$ in the power-law model, respectively. In the bottom panel, we plot $c(z_{\text{PM}} - z_{\text{PL}})$ in figure 3 again with the solid line. We can see that the spectroscopic data with Subaru/IRCS during the pericenter passage in 2018 play an important role to constrain the amount of the extended mass. (Color online)

us new information about the environment around Sgr A*. In this paper, we have discussed a dark mass distribution surrounding Sgr A* inside the orbit of S0-2 (within ~ 0.01 pc). The redshift of photons from S0-2 had varied from 4000 km s^{-1} to -2000 km s^{-1} during the pericenter passage in 2018, which is within 0.5 yr. This step variation gives a strong constraint on the dark mass distribution. We suggested a simple χ^2 analysis for the redshift of S0-2 to constrain the dark mass distribution and applied to the results in Saida et al. (2019). As a result, thanks to the step variation of the redshift during the pericenter passage in 2018, we can bound the amount of the extended mass inside the orbit of S0-2 less than 0.5% ($\sim 2 \times 10^4 M_\odot$) of the mass of Sgr A*. Our constraint is stronger by the factor 1/2 than the result in Gillessen et al. (2017) where the observational data in 2018 were not included. It means that the spectroscopic data during the pericenter passage in 2018 is crucial to give that strong constraint on the dark mass distribution. Furthermore,

our results are comparable to the results with the best-fitting parameter search to the motion of S0-2 including the data during the pericenter passage in 2018 (GRAVITY collab. 2018; Do et al. 2019; GRAVITY collab. 2020). By focusing on the steep variation in the time evolution of the redshift of S0-2 during the pericenter passage, we can give a constraint on the amount of the extended mass with less numerical costs. Although we consider both the power-law and the Plummer models as for the dark mass distribution, we do not find the significant difference between them.

Both the power-law and the Plummer models represent a stellar cluster surrounding Sgr A*. A dark matter distribution surrounding Sgr A* is also available and considered (Gondolo & Silk 1999; Sadeghian et al. 2013). The motion of S-stars can bound a dark matter profile. The amount of the dark matter within the orbit of S0-2 is a few % of the mass of Sgr A* at most (Hall & Gondolo 2006; Lacroix 2018). The observational data of S0-2 in 2018 were not included in these works. Because there is no significant difference between the mass profile functions of a stellar cluster and a dark matter models, the upper limit of the amount of the extended mass would be less than 1% of Sgr A* even if one considers a dark matter component.

In this paper, we have focused on the spectroscopic data of S0-2. The other observable is the astrometry of S0-2, and it gives us information about the dark mass distribution, of course. Rubilar & Eckart (2001) pointed out that the existence of dark mass distribution raises the apocenter shift even if in Newton's gravity. That is comparable to the relativistic apocenter shift if the amount of the extended mass is less than 1% of the mass of Sgr A*. Zakharov et al. (2007) studied how a dark matter profile affects the apocenter shift for S0-2 and showed that the astrometric observations could exclude some dark matter profiles. GRAVITY collab. (2019) considered a scalar field cloud surrounding Sgr A* as a dark matter model and studied the motion of S0-2. They showed that the motion of S0-2 is sensitive to the width of a dark matter cloud. It gives the range of the mass of the dark matter particle. Moreover, we can consider an exotic system that is without the central black hole, e.g., a dark matter core (Boshkayev & Malafarina 2019), a naked singularity (Dey et al. 2019). We can not exclude these alternatives in the present observations of S0-2. The χ^2 analysis suggested in this paper would be useful to give a constraint on these alternatives.

Recently, GRAVITY collab. (2020) reported that they had detected the pericenter shift for S0-2, which is consistent with the general relativity. S0-2 will experience the apocenter passage in 2026, and we expect to get new information through the event. Furthermore, Peißker, Eckart, and Parsa (2020) has found a new S-star moving inside the

orbit of S0-2, whose period is about 10yr. These new observational data would be useful to constrain on the dark mass distribution or to resolve the components of the dark mass distribution surrounding Sgr A* and to test alternatives for a black hole. For a research of a dark mass distribution surrounding Sgr A*, we should prepare a general relativistic dark mass model including the higher-order terms than the first post-Newtonian term. For example, if a geodesic represents the orbit of a star even for the case $M = M(r)$, we expect that new terms proportional to $\partial_r M$ appear in equation (1), which we do not introduce in this paper. $\partial_r M$ could be comparable with $(M - M_{\text{tot}})/r$, that is, the mass profile correction due to the dark mass. Therefore, it is worth including these new relativistic terms to evaluate the evolution of the star more precisely. We will investigate this issue in the near future.

Acknowledgments

Y. T. was supported by JSPS KAKENHI, Grant-in-Aid for Young Scientists (B) 26800150. S. N. was supported by JSPS KAKENHI, Grant-in-Aid for Challenging Exploratory Research 18K18760, and Grant-in-Aid for Scientific Research (A) 19H00695. T. O. was supported by JSPS KAKENHI, Grant-in-Aid for JSPS fellows JP17J00547. H. S. was supported by JSPS KAKENHI, Grant-in-Aid for Challenging Exploratory Research 26610050, and Grant-in-Aid for Scientific Research (B) 19H01900. M. T. was supported by DAIKO FOUNDATION, and JSPS KAKENHI, Grant-in-Aid for Scientific Research (C) 17K05439.

References

- Boehle, A., et al. 2016, *ApJ*, 830, 17
- Boshkayev, K., & Malafarina, D. 2019, *MNRAS*, 484, 3325
- Dey, D., Joshi, P. S., Joshi, A., & Bambhaniya, P. 2019, *International Journal of Modern Physics D*, 28, 1930024
- Do, T., et al. 2019, *Science*, 365, 664
- Genzel, R., et al. 2003, *ApJ*, 594, 812
- Ghez, A. M., et al. 2008, *ApJ*, 689, 1044
- Gillessen, S., Eisenhauer, F., Trippe, S., Alexander, T., Genzel, R., Martins, F., & Ott, T. 2009, *ApJ*, 692, 1075
- Gillessen, S., et al. 2017, *ApJ*, 837, 30
- Gondolo, P., & Silk, J. 1999, *Phys. Rev. Lett.*, 83, 1719
- GRAVITY collaboration 2018, *A&A*, 615, L15
- GRAVITY collaboration 2019, *MNRAS*, 489, 4606
- GRAVITY collaboration 2020, *A&A*, 636, L5
- Hall, J., & Gondolo, P. 2006, *Phys. Rev. D*, 74, 063511
- Iorio, L. 2011, *MNRAS*, 411, 453
- Lacroix, T. 2018, *A&A*, 619, A46
- Mouawad, N., Eckart, A., Pfalzner, S., Schödel, R., Moultaqa, J., & Spurzem, R. 2005, *Astronomische Nachrichten*, 326, 83
- Nishiyama, S., et al. 2018, *PASJ*, 70, 74

- Peißker, F., Eckart, A., & Parsa, M. 2020, *ApJ*, 889, 61
- Plummer, H. C. 1911, *MNRAS*, 71, 460
- Preto, M., & Saha, P. 2009, *ApJ*, 703, 1743
- Rubilar, G. F., & Eckart, A. 2001, *A&A*, 374, 95
- Sadeghian, L., Ferrer F., & Will, C. M. 2013, *Phys. Rev. D*, 88, 063522
- Saida, H., et al. 2019, *PASJ*, 71, 120
- Schödel, R., et al. 2007, *A&A*, 469, 125
- Zakharov, A. F., Nucita, A. A., de Paolis, F., & Ingrosso, G. 2007, *Phys. Rev. D*, 76, 062001